nature chemical biology

ARTICLE

PUBLISHED ONLINE: 13 JUNE 2016 | DOI: 10.1038/NCHEMBIO.2103

Small-molecule binding of the axin RGS domain promotes β-catenin and Ras degradation

Pu-Hyeon Cha[1,2,6], Yong-Hee Cho[1,2,6], Sang-Kyu Lee[1,2], JaeHeon Lee[1,2], Woo-Jeong Jeong[1,2], Byoung-San Moon[1,2], Ji-Hye Yun[1,3], Jee Sun Yang[1,2], Sooho Choi[1,3], Juyong Yoon[1,2], Hyun-Yi Kim[1,2], Mi-Yeon Kim[1,2], Saluja Kaduwal[1,2], Weontae Lee[1,3], Do Sik Min[1,4], Hoguen Kim[5], Gyoonhee Han[1,2] & Kang-Yell Choi[1,2]*

Both the Wnt/β-catenin and Ras pathways are aberrantly activated in most human colorectal cancers (CRCs) and interact cooperatively in tumor promotion. Inhibition of these signaling may therefore be an ideal strategy for treating CRC. We identified KY1220, a compound that destabilizes both β-catenin and Ras, via targeting the Wnt/β-catenin pathway, and synthesized its derivative KYA1797K. KYA1797K bound directly to the regulators of G-protein signaling domain of axin, initiating β-catenin and Ras degradation through enhancement of the β-catenin destruction complex activating GSK3β. KYA1797K effectively suppressed the growth of CRCs harboring *APC* and *KRAS* mutations, as shown by various *in vitro* studies and by *in vivo* studies using xenograft and transgenic mouse models of tumors induced by *APC* and *KRAS* mutations. Destabilization of both β-catenin and Ras via targeting axin is a potential therapeutic strategy for treatment of CRC and other type cancers activated Wnt/β-catenin and Ras pathways.

CRC is one of the most frequent cancers and the second leading cause of cancer-related deaths in Western countries[1]. The use of chemotherapy and molecular targeted therapy to treat CRC has increased overall survival[2]; however, the clinical benefits of these therapies are often short-lived and restricted to only a subpopulation of patients due to the development of acquired resistance through genetic mutations[3]. Therefore, additional effective therapies for treatment of human CRCs are needed.

CRC generally arises through the occurrence of multiple and sequential genetic abnormalities including adenomatous polyposis coli (*APC*) and *KRAS* mutations, which lead to aberrant activation of the Wnt/β-catenin and Ras/extracellular-signal-regulated kinase (ERK) pathways, respectively[4,5]. Mutations in *APC* are detected in over 90% of human CRCs, and these mutations promote the initiation of most CRCs[6]. *KRAS* mutations occur during early and intermediate stages of CRC tumorigenesis at a frequency of 32–57% and induce the progression of CRC[7,8]. Accumulating evidence shows that the Ras/ERK pathway strongly interacts with the Wnt/β-catenin pathway during the formation and growth of CRCs[9–11]. The oncogenic *Kras* mutation alone does not induce malignant transformation of the intestinal epithelium in mice; however, it accelerates tumorigenesis and confers invasive properties after *Apc* loss[9,12,13]. Based on the high frequency of concurrent *APC* and *KRAS* mutations and their strong cooperative interaction, therapies targeting both the Wnt/β-catenin and Ras/ERK pathways are suggested to be ideal treatments for human CRC[14–16]; however, therapeutics targeting both of these pathways have not been developed because the mechanisms regulating these pathways are not well understood.

Recently, we discovered that Ras proteins can be degraded by inhibition of the Wnt/β-catenin pathway via its negative regulators such as APC, axin and glycogen synthase kinase 3β (GSK3β)[16–19]. When the Wnt/β-catenin signaling is negatively regulated, the Ras degradation occurs together with the β-catenin degradation; Ras is phosphorylated by GSK3β, and β-TrCP E3 linker is subsequently recruited for ultimate proteasomal degradation[16]. Amounts of both β-catenin and Ras proteins are often increased in CRC, especially metastatic CRC involving cancer stem cell activation in both mice and humans[16,20]. The synergistic effect on tumor growth associated with mutations in both *APC* and *KRAS* is attributed to the stabilization of both β-catenin and oncogenic K-Ras by *APC* loss[16]. Based on our previous studies and with human tissue analyses[16,20], we screened a small-molecule library to identify compounds that destabilized both β-catenin and Ras proteins via inhibition of the Wnt/β-catenin pathway. We identified KY1220 and obtained its functionally improved derivative, KYA1797K. These compounds efficiently destabilized β-catenin and Ras, and they reduced the proliferation and transformation of various CRC cells harboring *APC* and *KRAS* mutations. We identified axin as a direct target for KYA1797K through *in vitro* binding studies, and uncovered details of the interaction between KYA1797K and regulators of the G-protein signaling (RGS) domain of axin using nuclear magnetic resonance (NMR) titration experiments. KYA1797K enhanced formation of the β-catenin destruction complex and induced GSK3β activation, leading to phosphorylation of both β-catenin and K-Ras at S33/S37/T41 and T144/T148 (ref. 16), respectively. Phosphorylated β-catenin and K-Ras were degraded via β-TrCP E3-linker-mediated polyubiquitinylation-dependent proteasomal degradation. We demonstrated the essential role of GSK3β in β-catenin and Ras degradations in experiments using *Gsk3b*$^{-/-}$ (here referred to as *Gsk3β*$^{-/-}$) mouse embryonic fibroblasts (MEFs), the K147A axin variant that is incapable of KYA1797K binding, or the K-Ras T144A/T148A variant in which the residues phosphorylated by GSK3β were abolished[16]. Finally, KYA1797K significantly ($P < 0.01$, Student's *t*-test) suppressed tumor growth and progression both in mouse xenografts of CRC cells harboring *APC* and *K-Ras* mutations and in an *Apc*$^{min/+}$/*Kras*^{G12D}*LA2* mouse model ($P < 0.01$, Student's *t*-test).

[1]Translational Research Center for Protein Function Control, Yonsei University, Seoul, Korea. [2]Department of Biotechnology, College of Life Science and Biotechnology, Yonsei University, Seoul, Korea. [3]Department of Biochemistry, College of Life Science and Biotechnology, Yonsei University, Seoul, Korea. [4]Department of Molecular Biology, College of Natural Science, Pusan National University, Pusan, Korea. [5]Department of Pathology, Yonsei University College of Medicine, Seoul, Korea. [6]These authors contributed equally to this work. *e-mail: kychoi@yonsei.ac.kr

Our study provides a new small-molecule-based approach for treatment of CRC and other cancer types with activated both Wnt/β-catenin and Ras-ERK pathways via degradation of both β-catenin and Ras. In addition, we identified axin as a target for our compound and elucidated its mode of action involving GSK3β activation via modulation of the β-catenin destruction complex.

RESULTS

Identification of a destabilizer of β-catenin and Ras

We have recently demonstrated that the Wnt/β-catenin signaling pathway regulates Ras protein stability and that Ras protein levels in CRC correlate with the level of Wnt/β-catenin signaling in mice and humans[16,20]. We determined Ras and β-catenin protein levels from two colon specimens from familial adenomatous polyposis (FAP) patients harboring an *APC* mutation that results in a truncated protein (**Supplementary Results**, **Supplementary Fig. 1a**,**b**) using immunoblotting and immunohistochemistry of fresh tissue. The levels of β-catenin and Ras were increased to a similar extent in tumors expressing wild-type (WT) or mutant (MT) *KRAS* compared with nontumor regions (**Fig. 1a** and **Supplementary Fig. 1c**). Based on those studies, we screened a small-molecule library to identify compounds that destabilize both β-catenin and Ras via inhibition of the Wnt/β-catenin pathway (**Supplementary Table 1** and **Supplementary Fig. 2a**). By screening compounds for their ability to inhibit (>90%) the TOPflash reporter activity stimulated by Wnt3a-conditioned medium (Wnt3a-CM) and then selecting compounds that destabilized both β-catenin and Ras without showing a toxic effect on neural stem cells (NSCs) (**Supplementary Fig. 2b**,**c**), we identified KY1220 (**1**; **Fig. 1b**), a compound showing a half-maximal inhibitory concentration (IC_{50}) of 2.1 μM in HEK293 reporter cells (**Supplementary Fig. 3a**). KY1220 dose-dependently decreased Wnt3a-CM-induced TOPflash reporter activation (**Supplementary Fig. 3b**) and mRNA expression of Wnt target genes *CCND1* and *MYC* in HEK293 cells (**Supplementary Fig. 3c**).

In HEK293 cells, both β-catenin and pan-Ras protein levels were similarly reduced in a dose-dependent manner after treatment with KY1220 (**Fig. 1c** and **Supplementary Fig. 3d**), whereas the mRNA levels of *CTNNB1* (which encodes β-catenin), *NRAS*, *KRAS* and *HRAS* remained unchanged (**Supplementary Fig. 3e**). We treated cells with KY1220 and proteasome inhibitors, and determined that the destabilization of Ras and β-catenin by KY1220 occurred via polyubiquitin-dependent proteasomal degradation (**Fig. 1d**,**e** and **Supplementary Fig. 3f**). K-Ras, which has a critical role in progression of CRCs, was also destabilized by KY1220 via polyubiquitin-dependent proteasomal degradation (**Supplementary Fig. 3g**). We observed that levels of both β-catenin and pan-Ras were reduced upon treatment with KY1220 in various CRC cell lines such as D-WT, D-MT (D-WT and D-MT cells express WT and MT K-Ras, respectively, in the DLD-1 genetic background[21]), HCT15, SW480 and LoVo cells (**Fig. 1f** and **Supplementary Fig. 3h**). KY1220 accelerated the degradation rates of both β-catenin and Ras in SW480 cell lines, as shown by measurements in the presence of cycloheximide (**Supplementary Fig. 3i**). Ras destabilization by KY1220 consequently inhibited the activities of both ERK and Akt, which are downstream effectors of Ras in SW480 cells harboring a *KRAS* mutation (**Fig. 1g**).

We evaluated the effects of KY1220 on proliferation and transformation in HCT15, SW480, D-WT and D-MT CRC cells. The proliferation and transformation of the cells were efficiently inhibited after treatment with KY1220 (**Fig. 1h** and **Supplementary Fig. 4a–c**). In contrast to its effect on CRC cell lines, KY1220 did not inhibit the growth of the normal human colonic fibroblast line CCD18-Co (**Supplementary Fig. 4d**).

Production of a KY1220 analog with improved functionality

To improve the activity and solubility of KY1220, we designed 150 analog compounds of it as a focused library for virtual screening (**Supplementary Fig. 5a** and **Supplementary Note**). Of the compounds, KYA1797 (**2**), KYA1690 (**3**) and KYA2370 (**4**) showed improved inhibition of the TOPflash activity compared to KY1220 (**Supplementary Fig. 5b**). These three compounds showed the best fit value on the generated pharmacophores (**Supplementary Fig. 5c**). The compounds each had one hydrophobic group on either their pyrrole or furan ring, and three hydrogen bond acceptors on the

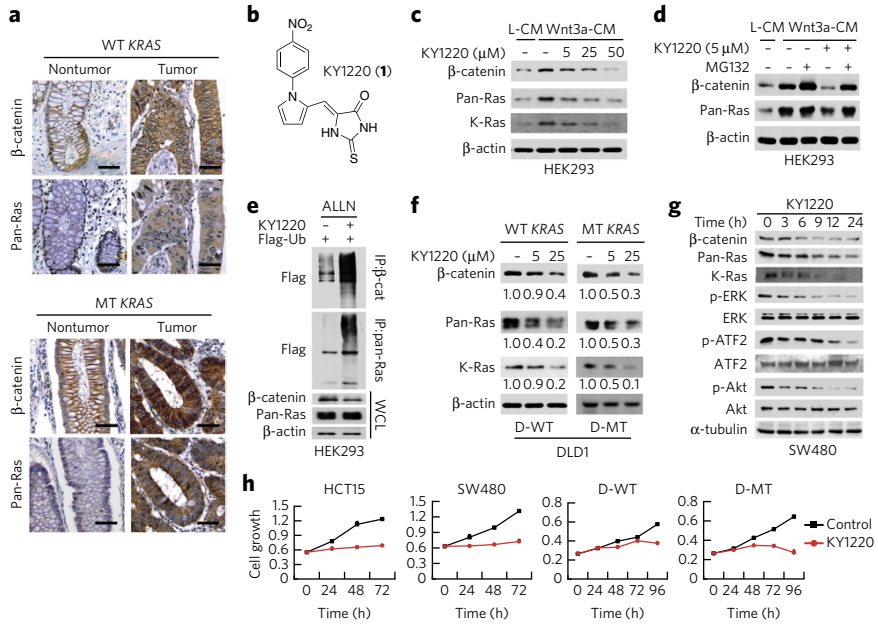

Figure 1 | Identification and characterization of KY1220, a small molecule that destabilizes both β-catenin and Ras. (**a**) Immunohistochemical analyses of β-catenin and pan-Ras in colon tissues from FAP patients expressing WT or MT *KRAS*. Scale bars, 50 μm. (**b**) Structure of KY1220. (**c**,**d**) Immunoblot analyses of proteasomal degradation of Wnt3a-CM-induced β-catenin, pan-Ras and K-Ras by KY1220 in HEK293 cells treated with L-cell-conditioned medium (L-CM) or Wnt3a-CM with indicated amounts of KY1220 (**c**) or with KY1220 with or without MG132 (**d**) for 8 h. (**e**) Immunoblot analyses of polyubiquitin-dependent proteasomal degradation of β-catenin (top) and pan-Ras (middle) KY1220 in HEK293 cells transfected with Flag-Ub and then treated with the proteasome inhibitor ALLN with or without KY1220 for 12 h. Whole-cell lysates (WCL) are shown at bottom. (**f**) Immunoblot analyses of D-WT and D-MT cell cultured with KY1220 for 24 h. Band intensities in all blots were analyzed using Image J, and values of the bands were normalized to the loading control protein β-actin. The relative densitometry values are presented below each blot as intensity ratios relative to experimental controls. (**g**) Immunoblot analyses of SW480 cells treated with KY1220 for indicated durations. (**h**) 3-(4,5-dimethylthiazol-2-yl)-2-5-diphenyltetrazolium bromide (MTT) assay of cell proliferation of HCT15, SW480, D-WT and D-MT cells treated with KY1220 or untreated (control) (mean ± s.d., $n = 3$). In **c**–**g**, WCL or immunoprecipitated samples were immunoblotted with antibodies to indicated proteins. All immunoblots are representative of two or more experiments. Full blot images for **Figure 1** and **Supplementary Figure 3** are shown in **Supplementary Figures 16** and **22**, respectively. The source data for **Supplementary Figures 2a**, **3a**,**b**,**e** and **4a–d** are provided in the **Supplementary Data**.

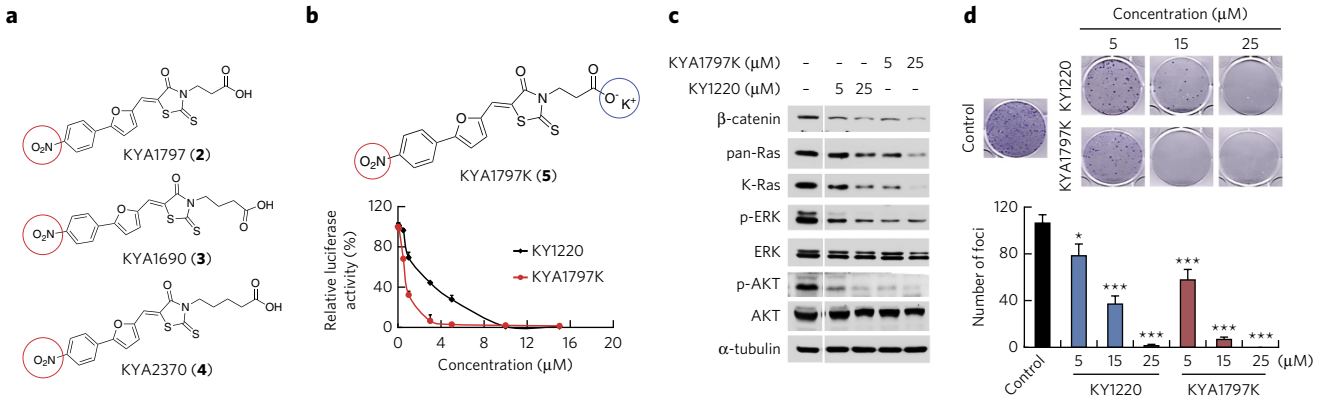

Figure 2 | Identification of KYA1797K, a derivative of KY1220 with improved inhibitory activity for Wnt/β-catenin signaling. (**a**) Structures of three derivatives of KY1220. Red circles highlight NO_2 residues, essential for inhibition of TOPflash activity. (**b**) Structure of KYA1797K; the potassium salt and the NO_2 are indicated by blue and red circles, respectively (top). Luciferase activity (normalized to Wnt3a-CM-treated control) in HEK293 reporter cells grown with indicated concentrations of KY1220 or KYA1797K in Wnt3a-CM for 18 h (bottom). The curves were used to determine the IC_{50} values for the inhibition of the TOPflash activity (mean ± s.d., $n = 3$). (**c**,**d**) Immunoblot analysis of the effect of KYA1797K and KY1220 on β-catenin and Ras degradation (**c**) and of inhibition of colony formation (**d**) in SW480 cells. Immunoblots are representative of two experiments; full blot images are shown in **Supplementary Figure 17**. The foci in **d** were photographed (top) and quantified (bottom; mean ± s.d.; $n = 3$). $^*P < 0.05$, $^{***}P < 0.001$ versus control; Student's *t*-test. The source data for **Supplementary Figures 5b**,**f** and **6** are shown in the **Supplementary Data**.

oxygen of 4-nitrophenyl, on the oxygen of rhodanine or thiohydantoin and on the oxygen of carboxylic acid (**Supplementary Fig. 5c**). Like KY1220, all three compounds had a NO_2 (**Fig. 2a**), indicating that the NO_2 at the *para* position of KY1220 is critical for its activity. For *in vivo* applications, we added a potassium salt (K) to each compound to improve its solubility and found that KYA1797K (5; **Fig. 2b**) was the only compound that dissolved in 10% Tween 80 and 90% phosphate-buffered saline (PBS), pH 7.4 (**Supplementary Fig. 5d**). Compared to KY1220, KYA1797K inhibited TOPflash activity to a greater extent (IC_{50} of KY1220 = 2.1 μM vs. IC_{50} of KYA1797K = 0.75 μM; **Fig. 2b**), and more effectively reduced the levels of both β-catenin and pan-Ras as well as the activities of ERK and Akt in

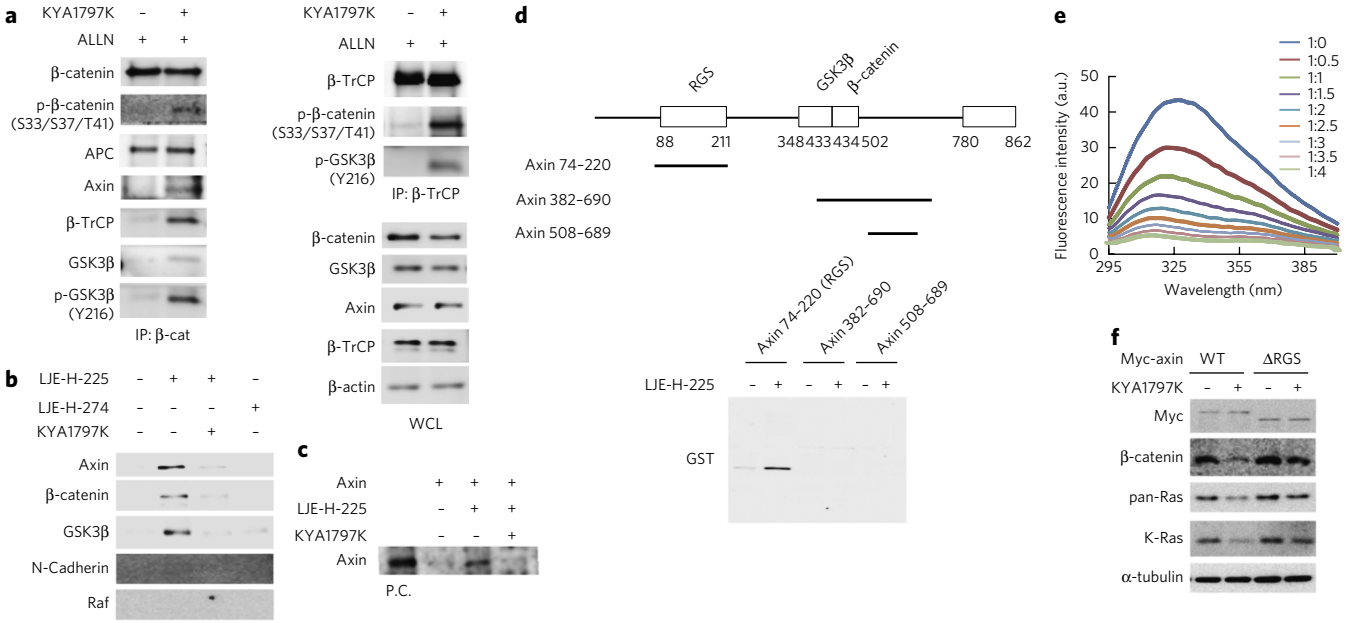

Figure 3 | Identification of a target protein of KYA1797K. (**a**) Immunoblots of immunoprecipitation (IP) with β-catenin antibodies (β-cat; left) or β-TrCP antibodies (top right) and of whole-cell lysates (WCL) from HEK293 cells treated with ALLN and with or without 25 μM KYA1797K for 12 h. Immunoblots are representative of three experiments; full blot images are shown in **Supplementary Figure 17**. (**b**) *In vitro* pulldown assay of HEK293 lysates (500 μg) with LJE-H-225 (100 μM) or LJE-H-274 (100 μM). KYA1797K (100 μM) was added to compete LJE-H-225-bound proteins. (**c**) *In vitro* pulldown assay of recombinant human axin (1 μg) with LJE-H-225 (100 μM). KYA1797K (100 μM) was added to compete with the axin-LJE-H-225 interaction, and axin (200 ng) was loaded as a positive control (P.C.). (**d**) Schematic of three axin fragments (left). *In vitro* pulldown assay of the glutathione-S-transferase (GST)-tagged axin fragments (300 μg each) with 100 μM of LJE-E-225 (right). (**e**) Fluorescence spectroscopy analysis of the interaction at indicated KYA1797K:axin74–220 molar ratios. a.u., absorbance units. (**f**) Immunoblot analysis of HEK293 cells transfected with pCS2-myc-axin (WT) or pCS2-myc-axin 207–832 (RGS) at 24 h after transfection with pAxin small interfering ((si)RNA), and subsequently treated with KYA1797K (25 μM) for 24 h. Immunoblots (**b**,**c**,**f**) are representative of two or more experiments; full blot images for **Figure 3** and **Supplementary Figures 7c** and **8a**,**b** are shown in **Supplementary Figures 18** and **23**, respectively. The source data for **Supplementary Figure 7b** is available in the **Supplementary Data**.

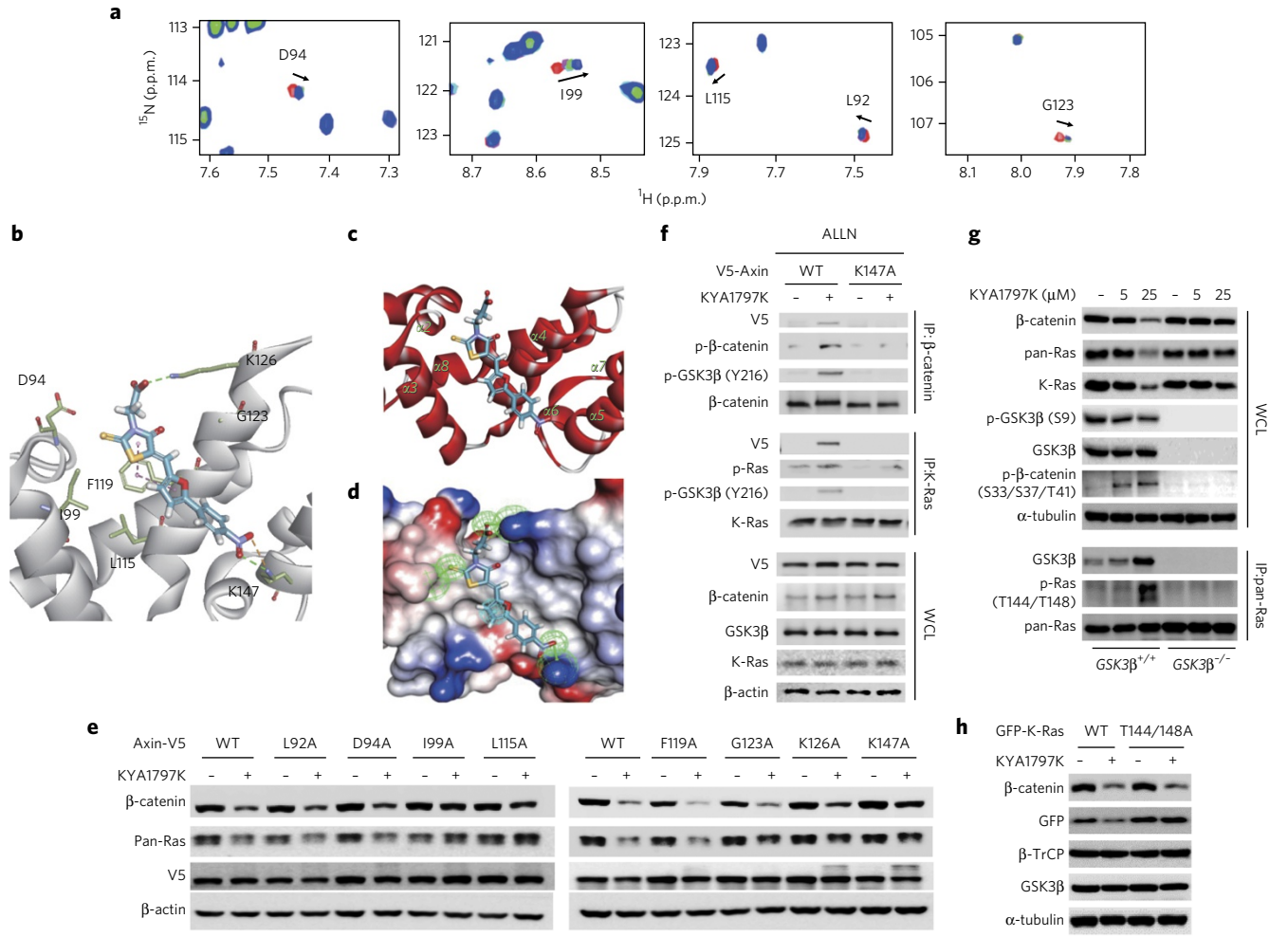

Figure 4 | Binding of KYA1797K to the axin-RGS domain, and its role in the degradation of β-catenin and Ras via GSK3β activation. (**a**) NMR titration for ^{15}N-labeled axin74–220 with KYA1797K. Titration points are indicated in red (1:0), magenta (1:1), cyan (1:2), green (1:3) and blue (1:4). A gradual perturbation in chemical shift is indicated by arrows. (**b**) Binding mode of KYA1797K-axin74–220 complex shown as a stick model. (**c**) Molecular docking model for NMR spectroscopy data represented by a ribbon diagram (Axin74–220, red; KYA1797K, blue). (**d**) Structure-based pharmacophore features of the axin-RGS-KYA1797K complex (cyan, hydrophobic group; green, hydrogen bond acceptor). The electrostatic surface of axin74–220 is shown in blue, positively charged; red, negatively charged; white, neural residues (**e**,**f**) Characterization of WT axin and its variants on β-catenin and Ras degradation by KYA1797K in HEK293 cells transfected with either pDEST40-axin1-V5 (WT) or the plasmid harboring a mutated *Axin* gene encoding the indicated variants with the V5 tag. After 24 h, the cells were treated with KYA1797K (25 μM) without (**e**) or with 25 μg/ml ALLN (**f**). (**g**) Effects of KYA1797K on β-catenin and Ras degradation in *Gsk3β*$^{+/+}$ and *Gsk3β*$^{-/-}$ MEFs. (**h**) Effects of KYA1797K on degradation of WT K-Ras or K-Ras-T144/148A, a GSK3β-mediated phosphorylation-deficient variant. HEK293 cells were transfected with either pEGFP-C3-K-Ras or pEGFP-C3-K-Ras-144A/T148A and incubated with KYA1797K (25 μM) for 24 h. Immunoblots (**e**–**h**) are representative of at least two experiments; full blot images for **Figure 4** and **Supplementary Figures 10**, **11a**,**b** and **14b** are available in **Supplementary Figures 18**, **19** and **24**. The source data for **Supplementary Figures 9** and **11c**–**f** are provided in the **Supplementary Data**.

SW480 cells (**Fig. 2c**). The reduction in colony formation was significantly larger with KYA1797K treatment compared with KY1220 treatment in both SW480 (**Fig. 2d**) and D-MT CRC cells (**Supplementary Fig. 5e**,**f**). Using multipathway reporter arrays, we found that KYA1797K significantly ($P < 0.01$, Student's *t*-test) decreased reporter activities for the Wnt/β-catenin and MAPK/ERK pathways but did not affect the reporter activities of other cancer-related pathways, such as the Notch and TGFβ pathways (**Supplementary Fig. 6**). These results indicate that KYA1797K selectively regulated the Wnt/β-catenin and Ras/ERK pathways.

KYA1797K binds to axin and destabilizes β-catenin and Ras

In previous studies, we have shown that the level of Ras protein is regulated by β-catenin destruction complex components, such as axin, APC or GSK3β[16–18]. KYA1797K enhanced the β-catenin binding affinity of endogenous axin, GSK3β and β-TrCP (**Fig. 3a**). Interaction between APC and β-catenin was not enhanced by KYA1797K, indicating that the compound had a specific effect in complex formation. KYA1797K stimulated binding of β-TrCP to β-catenin phosphorylated at S33, S37 and T41 by active GSK3β (phosphorylation at Y216) (**Fig. 3a**). These results indicated that KYA1797K promoted the formation of the β-catenin destruction complex. Therefore, we investigated β-catenin destruction complex components as potential targets for KYA1797K. To identify target proteins of KYA1797K, we generated a compound in which biotin was conjugated with the carboxylic acid group of KYA1797. However, the biotinylated compounds only weakly inhibited TOPflash activity. As an alternate approach, we generated active (LJE-H-225 (**6**)) and inactive (LJE-H-274 (**7**)) biotinylated 2,4-thiazolidinedione analogs with high solubility (**Supplementary Fig. 7a**). LJE-H-225 inhibited TOPflash activity with an IC_{50} value 9.2 μM (**Supplementary Fig. 7b**). We pulled down LJE-H-225-bound

proteins from HEK293 lysates, and confirmed by immunoblotting specific binding of LJE-H-225 to axin, β-catenin and GSK3β, but not N-Cadherin or Raf (**Fig. 3b**). Using purified recombinant proteins we found that axin, but not β-catenin or GSK3β, bound directly to LJE-H-225 (**Supplementary Fig. 7c**). We confirmed the specific binding of axin to LJE-H-225 by competition analysis using KYA1797K (**Fig. 3c**). In the axin mutant ΔEx4-9 (ref. 22), in which the GSK3β and β-catenin interaction is abolished, KYA1797K could neither enhance the GSK3β binding affinity for β-catenin and Ras, nor induce the subsequent polyubiquitinylation-mediated degradation of β-catenin and Ras (**Supplementary Fig. 8a**,**b**). In sum, these data demonstrated the importance of axin for mediating destabilization of β-catenin and Ras.

To determine the specific region of the axin protein required for interaction with LJE-H-225, we purified three bacterially expressed GST-fused axin fragments containing residues 74–220, 382–690 or 508–689 (**Fig. 3d**). Of these, LJE-H-225 uniquely bound to the axin fragment comprising residues 74–220 (axin74–220), which contains the regulator of G-protein signaling (RGS) domain (residues 88–211) (**Fig. 3d**). We confirmed the direct interaction between KYA1797K and the RGS domain of axin (axin-RGS) by a fluorescence assay (dissociation constant (K_d) of 2.9×10^{-7} M (**Fig. 3e**). Overexpression of axin lacking the RGS domain (ΔRGS) diminished the effect of KYA1797K on degradation of β-catenin and Ras relative to overexpressed WT axin (**Fig. 3f**).

To further characterize the interaction between axin-RGS and KYA1797K, we analyzed chemical shift perturbations using NMR spectra. We identified D94, I99, L115, L92 and G123 as amino acid residues involved in the binding of KYA1797K to the axin-RGS domain (**Fig. 4a**). Based on that result, we produced a modeled complex structure of axin-RGS domain and KYA1797K. The model showed that residues F119, K126 and K147 are involved in binding with KYA1797K: π-π stacking (F119), direct hydrogen bonding (K126 and K147) and electrostatic interactions (K147) (**Fig. 4b**). Our model predicted that K147 interacts with the nitro group of KYA1797K (**Fig. 2b**) through hydrogen bonding and electrostatic interaction (**Fig. 4b**). From the chemical shift perturbations and complex structure model, we localized the KYA1797K binding site to the axin-RGS domain surrounded by helixes 2, 3, 4 and 5 (α2, 3, 4 and 5), where the residues in the binding site contact KYA1797K through hydrophobic interactions and hydrogen bonding, which substantiates the pharmacophore hypothesis (**Fig. 4b–d**). To verify importance of the residues in the function of KYA1797K, we generated axin variants with L92A, D94A, I99A, L115A, F119A, G123A, K126A and K147A substitutions. Three variants (I99A, L115A and K147A) were less efficient than WT at degrading β-catenin and Ras in response to KYA1797K treatment (**Fig. 4e**). In accordance with our model's prediction that K147 interacts with the nitro group in KYA1797K, axin K147A was totally unresponsive to KYA1797K, as measured by the degradation of both β-catenin and Ras (**Fig. 4e**). KYA1797K showed critically reduced binding affinity to axin K147A in an *in vitro* binding analysis (K_d to WT axin-RGS = 2.9×10^{-7} M; K_d to axin K147A-RGS = 1.8×10^{-4} M, **Supplementary Fig. 9**). Binding of KYA1797K to the axin-RGS domain induced activation of GSK3β (phosphorylation at Y216) promoting phosphorylation of both β-catenin and K-Ras at S33, S37, T41 and T144 and T148 (ref. 16), respectively (**Fig. 4f**). However, the axin K147A variant did not induce these effects (**Fig. 4f**).

To demonstrate the importance of GSK3β in the KYA1797K-induced degradations of β-catenin and Ras, we treated *Gsk3β*$^{-/-}$ MEFs, in which neither β-catenin[23] nor Ras[16] can be phosphorylated by GSK3β, with KYA1797K. The compound did not induce degradation of β-catenin or Ras in the cells (**Fig. 4g**). The KYA1797K-induced degradation of both β-catenin and Ras was rescued only by the expression of WT GSK3β, not by the catalytically dead (KD) GSK3β variant, in the *Gsk3β*$^{-/-}$ MEFs (**Supplementary Fig. 10**). K-Ras T144A/T148A protein[16] was also not degraded in response to KYA1797K treatment (**Fig. 4h**), confirming that GSK3β-mediated phosphorylation was essential for Ras degradation as well as β-catenin degradation.

Tankyrase (TNKS) inhibitors (for example, IWR-1 (ref. 24) or XAV939 (ref. 25)) are known to suppress Wnt/β-catenin signaling pathway through axin stabilization. Unlike TNKS inhibitors, KYA1797K did not increase axin levels, and even slightly decreased them at concentrations of 25 μM in DLD1 and SW480 CRC cells (**Supplementary Fig. 11a**,**b**). We confirmed that neither IWR-1 nor XVA939 bound to the axin-RGS (**Supplementary Fig. 11c** vs. **Fig. 3e**), and KYA1797K did not inhibit the activity of TNKS 1 or 2 (**Supplementary Fig. 11d**). Although the mode of action of the TNKS inhibitors is different from that of

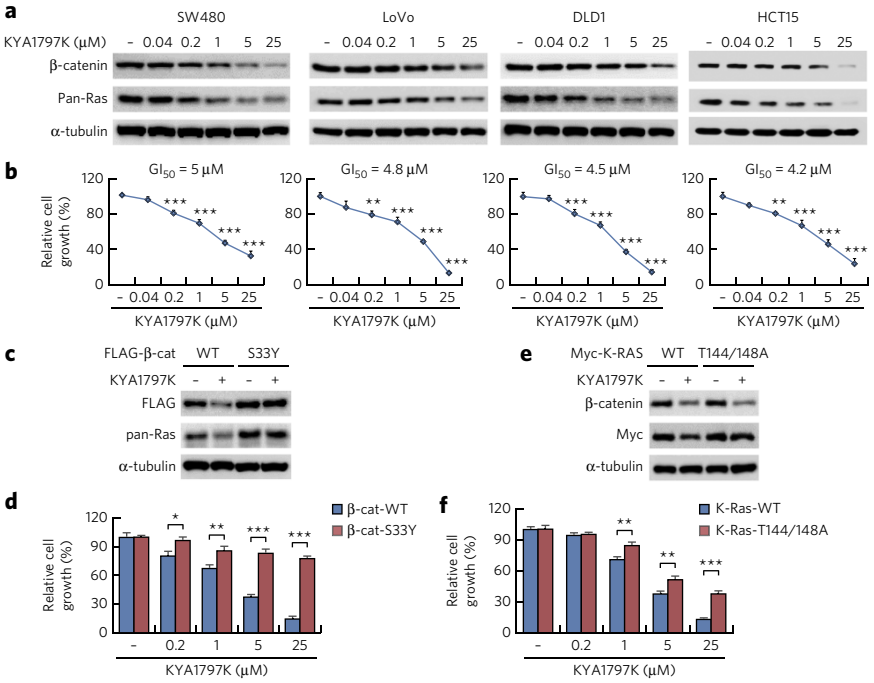

Figure 5 | Inhibitory effects of KYA1797K on cell proliferation via degradation of β-catenin and Ras. (**a**,**b**) Immunoblot analyses (**a**) and MTT assay to determine effects of KYA1797K on cell proliferation (**b**) of SW480, LoVo, DLD1 and HCT15 cells treated with KYA1797K for 24 h (**a**) or 4 d (**b**). In **b**, relative cell growth was normalized to DMSO-treated controls and 50% inhibition of growth (GI_{50}) was calculated (mean ± s.d., $n = 3$). $^{**}P < 0.01$ and $^{***}P < 0.001$; ANOVA. (**c**–**f**) Immunoblot analyses (**c**,**e**) and an MTT assay to determine effects of KYA1797K on cell proliferation (**d**,**f**) in DLD1 cells stably expressing WT β-catenin, S33Y β-catenin, WT K-Ras or T144/148A K-Ras treated with 25 μM KYA1797K for 24 h (**c**,**e**) or indicated concentrations for 4 d (**d**,**f**). The relative cell growth was normalized to DMSO-treated controls and data represent mean ± s.d. ($n = 3$). $^{*}P < 0.05$, $^{**}P < 0.01$ and $^{***}P < 0.001$; Student's *t*-test between WT and mutant forms of β-catenin (**d**) or K-Ras (**f**). Immunoblots (**a**,**c**,**e**) are representative of two or more experiments; full blot images are available in **Supplementary Figure 20**.

KYA1797K, the TNKS inhibitors also destabilized both β-catenin and Ras (**Supplementary Fig. 11a,b**). The destabilization of both β-catenin and Ras by the TNKS inhibitors increasing axin agreed with our previous studies showing an increase and a decrease of β-catenin and Ras levels by knock down and overexpression of axin, respectively[17]. Both β-catenin and Ras levels were reduced by treatment with TNKS inhibitors and KYA1797K; however, the kinetics of their decreases were different. The TNKS inhibitors did not show the clear dose dependency observed with KYA1797K treatment (**Supplementary Fig. 11a,b**). We also observed that KYA1797K and the TNKS inhibitors reduced colony formation (**Supplementary Fig. 11e,f**).

KYA1797K inhibited growth of CRC cells

We tested whether KYA1797K could inhibit cell proliferation by simultaneous destabilization of β-catenin and Ras in the CRC lines SW480, LoVo, DLD1 and HCT15. KYA1797K degraded both β-catenin and Ras in these cells in a dose-dependent manner (**Fig. 5a**). Consistent with these results, cell proliferation was suppressed by KYA1797K treatment (**Fig. 5b**). To confirm whether the anti-proliferative effect of KYA1797K was caused by destabilization of both β-catenin and Ras, we evaluated KYA1797K effects in DLD1 cells stably expressing WT β-catenin, WT K-Ras, β-catenin S33Y variant or K-Ras T144A/T148A variant[16]. KYA1797K destabilized β-catenin and Ras in DLD1 cells expressing WT β-catenin or WT K-Ras (**Fig. 5c,e**). However, the β-catenin S33Y and K-Ras T144A/T148A were not degraded by treatment with KYA1797K (**Fig. 5c,e**). Consistent with these observations, proliferation of DLD1 cells expressing WT β-catenin or WT K-Ras was efficiently inhibited by treatment with KYA1797K, whereas this inhibition was significantly weaker in the DLD1 cells expressing β-catenin S33Y or K-Ras T144A/T148A (**Fig. 5d,f**). The growth inhibition by KYA1797K was more significant in DLD-1 cells expressing K-Ras T144A/T148A compared to those expressing β-catenin S33Y, perhaps owing to continued β-catenin degradation in cells expressing K-Ras T144A/T148A (**Fig. 5c,e**). Our data indicated that KYA1797K inhibited proliferation of CRC cells mainly via destabilization of β-catenin with additional Ras degradation.

Antitumor effects of mutant *KRAS* and *APC*

To investigate the *in vivo* effects of KYA1797K, we injected the compound intraperitoneally (i.p.) into mice carrying xenografted tumors from the D-MT cell line that harbors both *APC* and *KRAS* mutations. KYA1797K administration (25 mg/kg) reduced both weight and volume of the tumor by 70% (**Fig. 6a,b**). To confirm the mechanism of KYA1797K action in tumor suppression, we assessed markers of the Wnt/β-catenin and Ras/ERK pathways and of proliferation. KYA1797K treatment significantly reduced levels of β-catenin and Ras proteins as well as Wnt/β-catenin and Ras signaling target, as shown by immunoblot (**Fig. 6c**) and immunohistochemistry analyses (**Fig. 6d**). We observed no change in the weight of (**Supplementary Fig. 12a**) and no abnormalities in liver tissues (**Supplementary Fig. 12b**) of mice treated with KYA1797K. These data suggest that KYA1797K suppressed the tumors induced by *APC* and *KRAS* mutations.

To investigate the anti-tumor effect of KYA1797K in a more pathophysiologically relevant system, we used *Apc*$^{min/+}$/*Kras*^{G12D}*LA2* mice, generated by crossing *Apc*$^{min/+}$ mice[26] with *Kras*^{G12D}*LA2* mice[27]. In contrast to *Apc*$^{min/+}$ mice, *Kras*^{G12D}*LA2* mice did not form tumors (**Supplementary Fig. 13a,b**), which is consistent with the requirement of *APC* loss for the initiation of CRC[6,13]. In *Apc*$^{min/+}$/*Kras*^{G12D}*LA2* mice, both tumor incidence and the number of tumors in the small intestine were higher than in *Apc*$^{min/+}$ mice (**Supplementary Fig. 13b,c**). KYA1797K treatment reduced the number of tumors in *Apc*$^{min/+}$/*Kras*^{G12D}*LA2* mice by 65% (**Fig. 6e,f** and **Supplementary Fig. 14a,b**). In *Apc*$^{min/+}$/*Kras*^{G12D}*LA2* mice treated with KYA1797K, the levels of β-catenin, pan-Ras, K-Ras, p-ERK, p-Akt, p-ATF2, c-Myc and PCNA were dramatically reduced compared with those for mice treated with vehicle (**Supplementary Fig. 14c**). The results of immunohistochemistry analyses were consistent with the biochemical results (**Fig. 6g**). Because nuclear β-catenin and membrane Ras are important for activation of the Wnt/β-catenin and Ras/ERK pathways, respectively, we observed localization of β-catenin and Ras after treatment with KYA1797K. KYA1797K

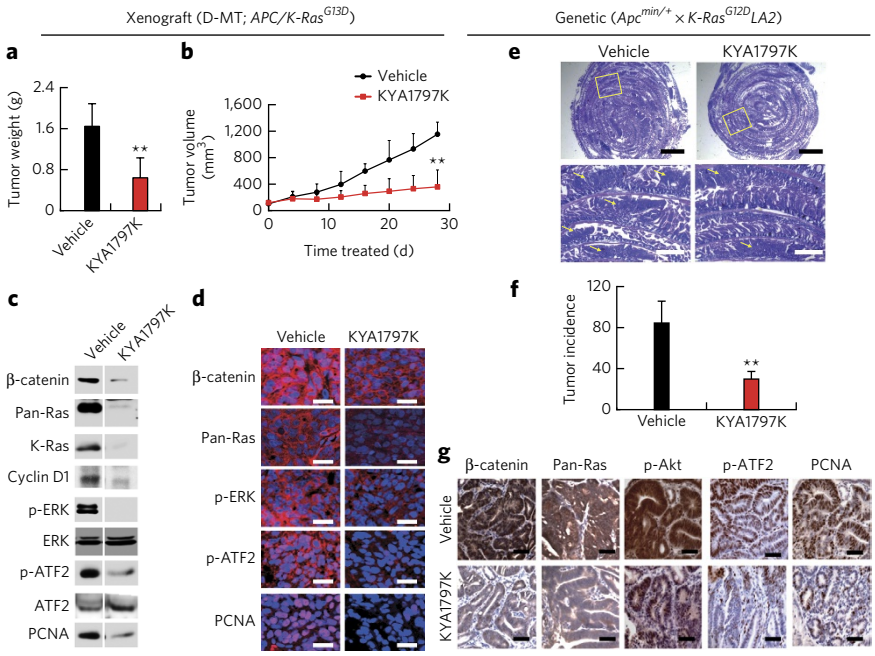

Figure 6 | Effects of KYA1797K on the growth of intestinal tumors harboring both *K-Ras* and *APC* mutations. (**a**–**d**) Analysis of D-MT cells injected subcutaneously into nude mice with subsequent intraperitoneal (i.p.) injection of vehicle or KYA1797K (20 mg/kg) for 28 d. Tumor weight (**a**) was measured at time of sacrifice and tumor volumes (**b**) of mice were measured every 4 d. Data represent mean ± s.d. (five mice per group). $^{**}P < 0.01$ for vehicle versus KYA1797K-treated tumors, by the Student's *t*-test. Immunoblot analyses of WCLs prepared from tumor tissues (**c**). Immunoblots are representative two experiments and the full blot images are shown in **Supplementary Figure 21**. Analysis of tissue sections incubated with the indicated antibodies; nuclei were counterstained with DAPI (**d**). Images were captured from non-hypoxic areas using an LSM510 confocal microscope. Scale bars, 20 μm. (**e**–**g**) Analysis of 5-week-old *Apc*$^{min/+}$/*Kras*^{G12D}*LA2* mice injected i.p. with vehicle or KYA1797K (25 mg/kg) 4 d per week for 7 weeks. Swiss roll images from the proximal areas containing the duodenum of the small intestine (**e**; H&E staining). Yellow boxes indicate enlarged areas in bottom images; arrowheads indicate tumors. Scale bars, 2 mm (top) and 500 μm (bottom). (**f**) Total incidence of tumors (mean ± s.d., four mice per group). $^{**}P < 0.01$ for vehicle versus KYA1797K-treated tumors; Student's *t*-test. (**g**) Immunohistochemistry analysis of tumor tissues treated with vehicle or KYA1797K. Scale bars, 80 μm. The source data for **Supplementary Figures 12a**, **13b,c** and **14b,d** are shown in the **Supplementary Data**.

significantly reduced the subcellular localization of β-catenin in the nuclei and pan-Ras on the membrane of tumor cells ($P < 0.001$, Student's *t*-test; **Supplementary Fig. 14d,e**). These data suggest that KYA1797K suppressed the formation and progression of small intestinal tumors in *Apc*$^{min/+}$/*Kras*^{G12D}*LA2* mice via inhibition of both β-catenin and Ras signaling.

DISCUSSION

Cancer development is primarily driven by multiple genetic mutations and molecular abnormalities rather than by a single defect[28,29]. Cancer treatments that inhibit a single target or pathway often have limited efficacy due to inherent redundancy or acquired resistance, which is caused by concomitant regulation of multiple signaling pathways to compensate for the inhibition[30]. Most CRCs arise through the mutation of multiple genes, including *APC*, *KRAS*, *SMAD4* and *TP53* (refs. 12,31). Of these genes, the *APC* (90%) and *KRAS* (32–57%) are frequently mutated in human CRCs, and the associated Wnt/β-catenin and Ras/ERK pathways have synergistic effects in the tumorigenesis of CRC[6,7,14,31]. Thus, targeting both the Wnt/β-catenin and Ras/ERK pathways may be an ideal therapeutic approach in human CRCs.

Here we identified and characterized KY1220 and its analog KYA1797K, which destabilized both β-catenin and Ras proteins, resulting in suppressed activation of Wnt/β-catenin, Ras/ERK and PI3K pathways. Although small molecules such as KYA1797K can suppress multiple pathways, KYA1797K did not inhibit other cancer-related pathways, including Notch, TGFβ and NF-κB, indicating target specificity. We identified axin as a target protein of KYA1797K and demonstrated that the axin RGS domain is critical for direct binding of KYA1797K. The RGS domain of axin is required for binding to APC[32]. TNKS inhibitors, including IWR-1 and XAV939, have been recently identified as Wnt/β-catenin pathway inhibitors that function via the stabilization of axin[24,25]. KYA1797K, unlike the TNKS inhibitors, directly binds the axin RGS domain and enhances formation of the β-catenin destruction complex, activating GSK3β. Although TNKS inhibitors degraded both β-catenin and Ras in DLD1 and SW480 cells, their degradation kinetics were different from those by KYA1797K. In addition, we did not observe clear dose dependency in degradation of β-catenin and Ras by TNKS inhibitors. The reason for the lack of TNKS inhibitor dose dependency is not clear;it may be attributable to the differences in the modes of action of the two different types of compounds. KYA1797K directly targeted axin and modulated conformation of the β-catenin destruction complex, whereas the TNKS inhibitors may change the stoichiometry of the complex components by increasing axin levels.

On the basis of the data described in this study, we suggest the following model for the action of KYA1797K in the degradation of β-catenin and Ras: by binding to the RGS domain of axin, KYA1797K enhanced formation of the β-catenin destruction complex that activates GSK3β (**Supplementary Fig. 15**); activated GSK3β phosphorylates both β-catenin and K-Ras at S33/S37/T41 and T144/T148 (ref. 16), respectively, and the phosphorylated proteins were degraded via β-TrCP E3 linker-mediated polyubiquitinylation-dependent proteasomal degradation[16] (**Supplementary Fig. 15**). Through inhibition of both Wnt/β-catenin and Ras/ERK pathways, KYA1797K significantly reduced proliferation of CRCs harboring *APC* and *KRAS* mutations both *in vitro* and *in vivo*. Therefore, our chemical approach appears to be a feasible strategy for finding small molecules that target both the Wnt/β-catenin and EGFR-Ras/ERK pathways. Optimization of the chemicals we identified by structure-based drug design and optimization for pharmacological aspects could lead to the discovery and development of new drugs for the treatment of human CRCs and other types of cancers with activated Wnt/β-catenin and/or Ras/ERK pathways.

Received 23 June 2015; accepted 25 March 2016; published online 13 June 2016

METHODS

Methods and any associated references are available in the online version of the paper.

References

1. Hawk, E.T. & Levin, B. Colorectal cancer prevention. *J. Clin. Oncol.* **23**, 378–391 (2005).
2. Jemal, A. *et al.* Cancer statistics, 2009. *CA Cancer J. Clin.* **59**, 225–249 (2009).
3. Waldner, M.J. & Neurath, M.F. The molecular therapy of colorectal cancer. *Mol. Aspects Med.* **31**, 171–178 (2010).
4. Chung, D.C. The genetic basis of colorectal cancer: insights into critical pathways of tumorigenesis. *Gastroenterology* **119**, 854–865 (2000).
5. Zhang, B. *et al.* β-Catenin and ras oncogenes detect most human colorectal cancer. *Clin. Cancer Res.* **9**, 3073–3079 (2003).
6. Kinzler, K.W. & Vogelstein, B. Lessons from hereditary colorectal cancer. *Cell* **87**, 159–170 (1996).
7. Bos, J.L. *et al.* Prevalence of ras gene mutations in human colorectal cancers. *Nature* **327**, 293–297 (1987).
8. Brink, M. *et al.* K-ras oncogene mutations in sporadic colorectal cancer in The Netherlands Cohort Study. *Carcinogenesis* **24**, 703–710 (2003).
9. Janssen, K.P. *et al.* APC and oncogenic KRAS are synergistic in enhancing Wnt signaling in intestinal tumor formation and progression. *Gastroenterology* **131**, 1096–1109 (2006).
10. D'Abaco, G.M., Whitehead, R.H. & Burgess, A.W. Synergy between Apc min and an activated ras mutation is sufficient to induce colon carcinomas. *Mol. Cell. Biol.* **16**, 884–891 (1996).
11. Luo, F. *et al.* Mutated K-ras(Asp12) promotes tumourigenesis in Apc(Min) mice more in the large than the small intestines, with synergistic effects between K-ras and Wnt pathways. *Int. J. Exp. Pathol.* **90**, 558–574 (2009).
12. Fearon, E.R. & Vogelstein, B. A genetic model for colorectal tumorigenesis. *Cell* **61**, 759–767 (1990).
13. Sansom, O.J. *et al.* Loss of Apc allows phenotypic manifestation of the transforming properties of an endogenous K-ras oncogene in vivo. *Proc. Natl. Acad. Sci. USA* **103**, 14122–14127 (2006).
14. Anastas, J.N. & Moon, R.T. WNT signalling pathways as therapeutic targets in cancer. *Nat. Rev. Cancer* **13**, 11–26 (2013).
15. Guardavaccaro, D. & Clevers, H. Wnt/beta-catenin and MAPK signaling: allies and enemies in different battlefields. *Sci. Signal.* **5**, pe15 (2012).
16. Jeong, W.J. *et al.* Ras stabilization through aberrant activation of Wnt/beta-catenin signaling promotes intestinal tumorigenesis. *Sci. Signal.* **5**, ra30 (2012).
17. Jeon, S.H. *et al.* Axin inhibits extracellular signal-regulated kinase pathway by Ras degradation via beta-catenin. *J. Biol. Chem.* **282**, 14482–14492 (2007).
18. Park, K.S. *et al.* APC inhibits ERK pathway activation and cellular proliferation induced by RAS. *J. Cell Sci.* **119**, 819–827 (2006).
19. Kim, S.E. *et al.* H-Ras is degraded by Wnt/beta-catenin signaling via beta-TrCP-mediated polyubiquitylation. *J. Cell Sci.* **122**, 842–848 (2009).
20. Moon, B.S. *et al.* Role of oncogenic K-Ras in cancer stem cell activation by aberrant Wnt/beta-catenin signaling. *J. Natl. Cancer Inst.* **106**, djt373 (2014).
21. Yun, J. *et al.* Glucose deprivation contributes to the development of KRAS pathway mutations in tumor cells. *Science* **325**, 1555–1559 (2009).
22. Arnold, H.K. *et al.* The Axin1 scaffold protein promotes formation of a degradation complex for c-Myc. *EMBO J.* **28**, 500–512 (2009).
23. Yost, C. *et al.* The axis-inducing activity, stability, and subcellular distribution of beta-catenin is regulated in *Xenopus* embryos by glycogen synthase kinase 3. *Genes Dev.* **10**, 1443–1454 (1996).
24. Chen, B. *et al.* Small molecule–mediated disruption of Wnt-dependent signaling in tissue regeneration and cancer. *Nat. Chem. Biol.* **5**, 100–107 (2009).
25. Huang, S.M. *et al.* Tankyrase inhibition stabilizes axin and antagonizes Wnt signalling. *Nature* **461**, 614–620 (2009).
26. Taketo, M.M. & Edelmann, W. Mouse models of colon cancer. *Gastroenterology* **136**, 780–798 (2009).
27. Johnson, L. *et al.* Somatic activation of the K-ras oncogene causes early onset lung cancer in mice. *Nature* **410**, 1111–1116 (2001).
28. Loeb, K.R. & Loeb, L.A. Significance of multiple mutations in cancer. *Carcinogenesis* **21**, 379–385 (2000).

29. Loeb, L.A., Loeb, K.R. & Anderson, J.P. Multiple mutations and cancer. *Proc. Natl. Acad. Sci. USA* **100**, 776–781 (2003).
30. Tortora, G. *et al.* Overcoming resistance to molecularly targeted anticancer therapies: Rational drug combinations based on EGFR and MAPK inhibition for solid tumours and haematologic malignancies. *Drug Resist. Updat.* **10**, 81–100 (2007).
31. Fearon, E.R. Molecular genetics of colorectal cancer. *Annu. Rev. Pathol.* **6**, 479–507 (2011).
32. Kikuchi, A. Roles of axin in the Wnt signalling pathway. *Cell. Signal.* **11**, 777–788 (1999).

Acknowledgments

We thank B. Vogelstein, K.W. Kinzler, J.-W. Oh, N.-C. Ha and E.-h. Jho for providing cells and reagents. This work was supported by the National Research Foundation of Korea (NRF) grant funded by the Korean Government (MSIP) (grants 2016R1A5A1004694, 2015R1A2A1A05001873). Y.-H.C. and S.C. were supported by a BK21 studentship from the NRF.

Author contributions

P.-H.C., Y.-H.C., S.-K.L., W.-J.J., B.-S.M., J.-H.Y., S.C., J.Y., M.-Y.K. and S.K. designed and performed the all experiments. J.L. and J.S.Y. synthesized chemicals. P.H.C., J.S.Y., H.-Y.K., D.S.M., H.K., W.L. G.H. and K.-Y.C. performed data analysis. P.-H.C., Y.-H.C., J.Y., J.S.Y., D.S.M., G.H. and K.-Y.C. wrote the manuscript.

Competing financial interests

The authors declare no competing financial interests.

Additional information

Any supplementary information, chemical compound information and source data are available in the online version of the paper. Reprints and permissions information is available online at http://www.nature.com/reprints/index.html. Correspondence and requests for materials should be addressed to K.-Y.C.

ONLINE METHODS

Cell culture, transfection and drug treatment. HEK293 cells, human CRC cells (HCT15, SW480, LoVo and DLD1), and CCD18-Co cells were obtained from the American Type Culture Collection (ATCC). HEK293 reporter cells[33] (HEK293 cells containing the chromosomally incorporated TOPflash gene) were provided by S. Oh (Kuk Min University, Korea). Isogenic human DLD-1 CRC cell lines expressing either WT or MT *KRAS* (D-WT and D-MT cells, respectively)[21] were provided by B. Vogelstein (Johns Hopkins Oncology Center). Immortalized *Gsk3β*$^{+/+}$ and *Gsk3β*$^{-/-}$ MEFs were provided by J. Woodgett (Mount Sinai Hospital–Samuel Lunenfeld Research Institute, Canada), and these cells were maintained as previously described[34]. HEK293 cells, HEK293 reporter cells and LoVo cells were cultured in DMEM (Gibco) supplemented with 10% FBS (FBS; Gibco). HCT15, SW480, DLD1, and the isogenic D-WT and D-MT cells were maintained in RPMI 1640 medium (Gibco) containing 10% FBS. CCD18-Co cells[35] were grown in DMEM supplemented with 20% FBS and 1× nonessential amino acids (Sigma-Aldrich). Mycoplasma contamination tests were performed for all cells which used in this study. Wnt3a-CM and L-CM were prepared as previously described[33]. For the generation of stable cell lines, DLD1 cells were transfected with FLAG-WT-β-catenin-pcDNA3.0, FLAG-S33Y-β-catenin-pcDNA3.0, pcDNA3.1-WT-K-Ras-myc or pcDNA3.1-T144/148A-K-Ras-myc[16], and were selected in a medium containing geneticin (G418; Gibco). Lipofectamine (Invitrogen) was used for plasmid transfection, according to the manufacturer's instructions. All chemicals were dissolved in dimethyl sulfoxide (DMSO; Sigma-Aldrich) for the *in vitro* studies. When indicated, ALLN (25 μg/ml; Sigma-Aldrich) or MG132 (20 μM; AMRESCO) were added to media to inhibit protein degradation. To inhibit protein synthesis, 100 μg/ml of cycloheximide (Sigma-Aldrich) was used.

Screening for compounds that destabilize both β-catenin and Ras. To identify small molecules that destabilize both the β-catenin and Ras proteins via inhibition of Wnt/β-catenin signaling, compounds that inhibit the TOPflash activity were initially selected by screening chemical libraries (~3,599 compounds; Chemdiv and Sigma LOPAC 1280) in HEK293 reporter cells. For screening, HEK293 reporter cells were seeded into 96-well black polystyrene plates (Greiner Bio-One) at 1.5×10^4 cells per well and cultured for 18 h. Each compound in the chemical library or control (DMSO) with Wnt3a-CM was then added to the wells at a final concentration of 10 μM. After 18 h, the plates were assayed for firefly luciferase activity[33]; relative reporter activity was determined after the data were normalized relative to the Wnt3a-CM control. In total, 40 compounds exhibiting >90% inhibition of reporter activity were selected.

To identify compounds that reduce the abundance of both endogenous β-catenin and Ras proteins, HEK293 cells were grown to a density of 2×10^5 cells/well in 6-well plates and then treated with each compound at a concentration of 10 μM in medium containing Wnt3a-CM. Compounds that reduced the levels of both β-catenin and Ras were identified by immunoblotting analyses of WCLs. We identified 21 compounds that reduced the abundance of both β-catenin and Ras in treated cells. To check cellular toxicity of compounds, NSCs were extracted from the forebrain of E14.5 rats[36] and maintained in an undifferentiated state by culturing in medium containing 10 ng/ml of bFGF (Peprotech). Undifferentiated NSCs (1×10^5) were treated with of each compound (10 μM) and cell morphology was assessed by capturing black and white images of the cells after 48 h. Seven compounds that induced apoptotic cell morphology in highly fragile primary NSCs were disregarded (**Supplementary Fig. 2c**). Summary of high-throughput screening results is provided in **Supplementary Table 1**.

Reporter assay. A total of 5×10^4 HEK293 reporter cells were seeded into triplicate wells of a 24-well plate. The cells were treated with Wnt3a-CM or L-CM in combination with individual compounds at 10 μM and cultured for 18 h. The cells were then harvested and lysed in 60 μl of Reporter Lysis Buffer (Promega) according to the manufacturer's instructions. After centrifugation, 20 μl of the supernatant was used to measure luciferase activity. Relative luciferase activities were normalized to that of the Wnt3a-CM control.

Immunoblotting. Cells were washed in ice-cold PBS (Gibco) and lysed using radio-immunoprecipitation assay (RIPA) buffer (Millipore). Samples of mice tissues stored in liquid nitrogen were prepared in RIPA buffer and then were homogenized. Proteins were separated on a 6–15% sodium dodecyl sulfate (SDS) polyacrylamide gel and transferred to a nitrocellulose membrane (Whatman). Immunoblotting was performed with the following primary antibodies: anti-pan-Ras monoclonal (clone Ras10, Millipore, MABS195; 1:3,000), anti-β-catenin (Santa Cruz Biotechnology; sc-7199; 1:3,000), anti-c-Myc (Santa Cruz Biotechnology, sc-789; 1:1,000), anti-p-ATF-2 (Cell Signaling Technology, #9221S; 1:1,000), anti-ATF2 (Santa Cruz Biotechnology, sc-6233; 1:1,000), anti-p-ERK (Cell Signaling Technology, #9101S; 1:1,000), anti-ERK (Santa Cruz Biotechnology, sc-514302; 1:10,000), anti-p-Akt (Cell Signaling Technology, #4060S; 1:1,000), anti-AKT (Santa Cruz Biotechnology, sc-8312; 1:3,000), anti-PCNA (Santa Cruz Biotechnology, sc-56; 1:1,000), anti-cyclin D1 (Santa Cruz Biotechnology, sc-450; 1:500), anti-β-actin (Santa Cruz Biotechnology, sc-47778; 1:5,000), anti-Flag (Cell Signaling Technology, #2368; 1:3,000), anti-K-Ras (Santa Cruz Biotechnology, sc-30; 1:1,000), anti-APC (Santa Cruz Biotechnology, sc896; 1:3,000), anti-axin (Millipore Corporation, #06-022; 1:1,000), anti-p-β-catenin (S33/S37/T41; Cell Signaling Technology, #9561S; 1:1,000), anti-β-TrCP (Cell Signaling Technology, #4394S; 1:2,000), anti-GSK3β (Cell Signaling Technology, #9315S; 1:3,000), anti-p-GSK3β (Y216; BD Bioscience, #612313; 1:1,000), anti-p-GSK3β (S9; Cell Signaling Technology, #9336S; 1:1,000), anti-V5 (MBL International., M167-3; 1:3,000), anti-N-cadherin (BD Bioscience, #610920; 1:1,000), anti-Raf (Santa Cruz Biotechnology, sc-7267; 1:1,000), anti-Myc (Santa Cruz Biotechnology, sc-40; 1:3,000), anti-Flag (Sigma-Aldrich, F7425; 1:1,000), anti-HA (Cell Signaling Technology, #2367S; 1:1,000), anti-GST (Millipore, 06-332; 1:1,000), anti-GFP (Applied Biological Materials INC., G096; 1:3,000) and anti-α-tubulin (Cell Signaling Technology, #3873S; 1:10,000). The anti-p-Ras antibody (1:1,000) which recognizes phosphorylation of Ras proteins at T144 and T148 were described in our previous study[16]. Horseradish-peroxidase-conjugated anti-mouse (Cell Signaling Technology, #7076; 1:3,000) or anti-rabbit (Bio-Rad, #1706515; 1:3,000) secondary antibodies were used. The full blot images for all immunoblotting are shown in **Supplementary Figures 16–24**.

Immunoprecipitation and ubiquitination assays. Immunoprecipitation and *in vivo* ubiquitination assays were performed as previously described[19]. Briefly, cells were washed in ice-cold PBS and lysed with RIPA buffer. For the *in vivo* ubiquitination assays, N-ethylmaleimide (Sigma-Aldrich; 10 mM) was subsequently added to the RIPA buffer. WCLs were incubated with pan-Ras and protein G agarose beads (Thermo Scientific) or β-catenin and protein A agarose beads (Thermo Scientific) at 4 °C for 12 h, and the beads were then washed 3 times in RIPA buffer. The resulting immune complexes were resolved by SDS-PAGE, and immunoblotting was performed with the indicated antibodies.

Plasmids. The plasmid pCS4-3xFlag-Ub was the gift of D.-W. Kim (Yonsei University, Korea). Plasmids pGEX-TEV-axin74-220, pGEX-TEV-axin275-684 and pGEX-TEV-axin435–681 were provided by N-C. Ha[37] (Pusan National University). Myc-WT-axin and Myc-ΔRGS axin (residues 207–832) were provided by E.-h. Jho[38] (University of Seoul). Plasmid pAxin-siRNA, which was used for axin knockdown, was described in a previous study[17]. FLAG-WT-β-catenin-pcDNA3.0 and FLAG-S33Y-β-catenin-pcDNA3.0 (ref. 39) were provided by E.R. Fearon (University of Michigan). pDEST40-Axin1 and pDEST40-AxinΔEx4-9 were provided by R.C. Sears[22] (Oregon Health and Science University) and mutagenesis methods in the axin-RGS domain are described in Online Methods and in **Supplementary Table 2**. Substitution of theronines 144 and 148 to alanines (T144/148A) in oncogenic K-Ras12V, which are conserved phosphorylation sites of H-Ras (NM_001130442.2) was performed with pEGFP-C3–K-Ras and pcDNA3.1-WT-K-Ras-myc[16] by using the Quikchange site-directed mutagenesis method (Stratagene). Mutagenesis primers and PCR conditions were as follows; forward, 5′-TTTATTGAAGCAT CAGCAAAGGCAAGACAGGGT-3′; reverse, 5′-ACCCTGTCTTGCCTTTGC TGATGCTTCAATAAA-3′; 19 cycles of 30 s at 95 °C, 60 s at 55 °C, and 15 min at 72 °C. PCR products were treated with the restriction endonuclease DpnI (Enzynomics), and transformed into competent DH5α cells. pTOPFLASH and pFOPFLASH[18] were used for reporter assays with the pCMV–β-galactosidase reporter (Clontech). The pCMV-WT-GSK3β-HA and pCMV-KD-GSK3β-HA (catalytically inactive K85A form) plasmids were provided by J. Chung (Seoul National University).

Cell proliferation and colony formation assays. To assay cell proliferation, HCT15 or SW480 cells were plated at a density of 2×10^4 cells/well, and D-WT or D-MT cells were seeded at a density of 1×10^4 cells/well in a 24-well plate. The cells were then treated with 25 μM KY1220 or KYA1797K or with control

(DMSO) for 72 h. In a 96-well plate, cells were seeded at a density of 3×10^3 cells/well. After 24 h, the cells were treated with KY1220, KYA1797K, IWR-1 or XAV939 for 4 d. Next, 3-(4,5-dimethylthiazol-2-yl)-2-5-diphenyltetrazolium bromide (MTT; AMRESCO) reagent was added to each well at a concentration of 0.25 mg/ml. After incubation for 2 h at 37 °C, insoluble purple formazan was obtained by removing the medium and incubating in 1 ml (24-well) or 200 µl (96-well) of DMSO for 1 h. The absorbance of the formazan product was determined at 590 nm every 24 h.

For colony formation assays, cells were seeded in 6- or 12-well plates (500 cells/well for HCT15, SW480, D-WT and D-MT cells). The cells were treated with control (DMSO), KY1220, KYA1797K, IWR-1 or XAV939 with medium changes every 3 d until visible colonies formed. At the end of the experiment, cells were fixed in 4% paraformaldehyde (PFA) for 30 min and stained with 0.5% crystal violet in 20% ethanol for 30 min.

Mouse xenograft assay. All animal experiments were performed in accordance with Korean Food and Drug Administration guidelines. Protocols were reviewed and approved by the Institutional Review Board of Severance Hospital, Yonsei University College of Medicine. Approximately 4- to 6-week-old male athymic BalbC *nu/nu* mice were purchased from Slc Inc. (Shizuoka). Mice were housed in microventilation cage system (MVCS) cages with a computerized environmental control system (Threeshine Inc.). The temperature was maintained at 24 °C with a relative humidity of 45–55%. The mice were provided a standard maintenance diet (Dae Han Bio Link). After acclimatization for 1 week, the mice were injected subcutaneously in the dorsal flank with 5×10^6 D-MT cells in 100 µl of PBS:Matrigel (BD Bioscience; 2:1). When the mean tumor size reached between 100–200 mm^3, the mice were randomly divided into two groups (vehicle-treated and KYA1797K-treated groups; 5 male mice per group). KYA1797K (in a suspension of 90% PBS and 10% Tween 80) was injected i.p. 5 d per week at a dose of 20 mg/kg. Tumor volume and body weight were measured every 4 d. Tumors were measured using Vernier calipers, and tumor volume was calculated according to the following formula: $\pi/6 \times$ length $\times$ width $\times$ height. Mice were killed when the tumor volume exceeded 1,200 mm^3. Twenty-eight days after drug treatment, the mice were killed, and the tumors were excised, weighed, and fixed in 4% PFA or snap-frozen in liquid nitrogen for further analysis.

Animal models and analysis of tumor tissue. C57BL/6J-*Apc*$^{Min/+}$ (*Apc*$^{min/+}$), B6.129S-*Kras*^{tm3Tyj} (*Kras*^{G12D}*LA2*), and C57BL/6J-*Apc*^{1638N}(*Apc*^{1638N}) mice were obtained from Jackson Laboratory or the National Cancer Institute mouse repository. To generate *Apc*$^{min/+}$/*Kras*^{G12D}*LA2* and *Apc*^{1638N}/*Kras*^{G12D}*LA2* mice, *Apc*$^{min/+}$ and *Apc*^{1638N} mice were crossed with *Kras*^{G12D}*LA2* mice, respectively. Mouse genotyping was performed using genomic DNA extracted from the tail, and we used male mice for further animal experiments. The mice were randomly assigned to two groups receiving either vehicle or KYA1797K.

To investigate the *in vivo* efficacy of KYA1797K, 5-week-old WT (C57BL/6J$^{+/+}$; $n = 5$), *Apc*$^{min/+}$ ($n = 6$), *Kras*^{G12D}*LA2* ($n = 5$), and *Apc*$^{min/+}$/*Kras*^{G12D}*LA2* ($n = 4$) mice were injected i.p. with KYA1797K (25 mg/kg) 4 d per week for 7 weeks. Immediately after sacrifice, the abdomen of each mouse was cut open longitudinally and cleaned by flushing with PBS. Proximal regions of the small intestine were dissected, stained with 0.025% methylene blue (Sigma-Aldrich) for 2 min, and fixed with 4% PFA. Gross images of tumor tissues were captured, and the tissues were resected and embedded in paraffin according to standard procedures. The tumors were classified according to standard World Health Organization histopathological criteria. Medium and large size tumors were classified based on a diameter of over 2 mm and over 3 mm, respectively. For histopathologic analyses, a subset of freshly isolated tissues were snap-frozen in liquid nitrogen and stored at −80 °C. To confirm the effects of KYA1797K *in vivo*, KYA1797K (25 mg/kg) or vehicle was injected i.p into 11-week-old male *Apc*^{1638N}/*Kras*^{G12D}*LA2* mice for 1 week, and ALLN was injected 9 h before euthanasia. Tumors in *Apc*^{1638N}/*Kras*^{G12D}*LA2* mice were frozen in liquid nitrogen until analysis.

Immunohistochemistry (IHC). For IHC analysis, 4-µm paraffin-embedded tissue sections were treated with citrate buffer (pH 6.0) and autoclaved for 15 min. To block endogenous peroxidase activity before peroxidase IHC analysis, tissues were incubated with 0.345% H_2O_2 (Samchun Chemicals) for 30 min. The sections were then blocked with 5% bovine serum albumin (BSA) and 1% normal goat serum (NGS; Vector Laboratories) in PBS for 30 min or in 10% BSA and 1% NGS in PBS for 1 h for mouse tumor samples. For fluorescence IHC, sections were incubated overnight at 4 °C with the following primary antibody: anti-β-catenin (BD Bioscience, #610154; 1:200), anti-pan-Ras monoclonal (clone Ras10, Millipore, MABS195; 1:100), anti-p-ERK (Cell Signaling Technology, #9101S; 1:100), anti-p-ATF-2 (Cell Signaling Technology, #9221S; 1:100), anti-PCNA (Santa Cruz Biotechnology, sc-56; 1:250), anti-p-Akt (Cell Signaling Technology, #4060S; 1:250). Then, the sections were incubated with anti-mouse Alexa Fluor 488 (Life Technologies, A11008; 1:500) or anti-rabbit Alex Fluor 555 (Life Technologies, A21428; 1:500) secondary antibodies for 1 h at room temperature. The sections were then counterstained with 4′, 6-diamidino-2-phenylindole (DAPI; Sigma-Aldrich) and mounted in Gel/Mount media (Biomeda Corporation). All incubations were conducted in dark, humid chambers. The fluorescence signal was visualized using a confocal microscope (LSM510; Carl Zeiss) at excitation wavelengths of 488 nm (Alexa Fluor 488), 543 nm (Alexa Fluor 555) and 405 nm (DAPI). At least three fields per section were analyzed. For peroxidase IHC analysis, before incubating sections with mouse primary antibody, mouse IgG was blocked using a M.O.M Mouse IgG blocking kit (Vector Laboratories). Sections were incubated with primary antibody overnight at 4 °C, followed by incubation with biotinylated anti-mouse (Dako, E-0433; 1:300) or biotinylated anti-rabbit (Dako, E-0353; 1:300) secondary antibodies for 1 h at room temperature. The samples were then incubated in avidin-biotin complex solutions (Vector Laboratories), stained with 3, 3′-diaminobenzidine (DAB; Dako) for 3–7 min and counterstained with Mayer's hematoxylin (Muto). All incubations were conducted in humid chambers. Signals were analyzed using a bright field microscope (Nikon TE-2000U). Expression of β-catenin or pan-Ras as indicated in IHC images was quantified using HistoQuest software (TissueGnostics) from representative images. All signals were analyzed in a double-blinded manner.

Biotinylated chemical affinity pulldown. HEK293 cells were lysed in lysis buffer (20 mM Tris-HCl pH 7.5, 150 mM NaCl, 1% NP-40, 2 mM EDTA and protease inhibitors; Sigma-Aldrich). Lysates were incubated with/without biotinylated chemicals (100 µM) together with streptavidin beads (Thermo Scientific) at 4 °C overnight. For competition experiments, KYA1797K (100 µM) was added to the mixture. After incubation, the affinity matrix was washed six times with cold lysis buffer, and the bound proteins were analyzed by immunoblotting. For direct binding analysis, human recombinant axin1 (OriGene Technologies, Inc.), GSK3β (USBiological) or β-catenin was incubated as described above. Recombinant β-catenin proteins were purified from *Escherichia coli* C41 transformed with pGEX4T3-β-catenin as described previously[16]. To narrow down the binding site of KYA1797K in axin, three GST-tagged axin fragments (residues 74–220, 275–684 and 435–681) were prepared as described previously[37], and the proteins were assayed by affinity pull-down with LJE-H-225 as described above.

Protein expression and purification for NMR spectroscopy and fluorescence experiments. The gene encoding axin74–220 was amplified by PCR from the full-length axin cDNA (NM_003502.3) using complementary primer pairs and then cloned into pET32a (Novagen), an *E. coli* expression vector incorporating sequences encoding a hexa-histidine affinity tag and the tobacco etch virus (TEV) protease recognition site (ENLYFQG). Mutagenesis of the codon encoding lysine 147 to alanine (K147A) in axin was done according to the Quikchange site-directed mutagenesis method (Stratagene). The cloning results were confirmed by DNA sequencing (Cosmogenetech.co). The recombinant plasmid was transformed into *E. coli* BL21 (DE3). Cells were cultured in M9 minimal medium with ampicillin (100 µg/ml) at 37 °C until reaching an optical density at 600 nm of about 0.7, at which time IPTG was added to a concentration of 0.5 mM, and the cells were cultured for an additional 18 h at 18 °C. Cells were harvested via centrifugation (6,000*g* for 30 min, 4 °C). For NMR spectroscopy experiments, ^{15}N-, $^{13}C/^{15}N$ uniformly labeled proteins were cultivated in minimal medium with $^{15}NH_4Cl$, U-^{13}C6-glucose. Harvested cells were disrupted by sonication in lysis buffer consisting of 25 mM sodium phosphate (pH6.8), 300 mM sodium chloride, 20 mM β-mercaptoethanol, and

doi:10.1038/nchembio.2103

protease inhibitor cocktail (Roche). The hexa-histidine-tagged fusion proteins were purified via immobilized metal affinity chromatography on a Ni-NTA column (Amersham Pharmacia) and cleaved for 15 h in batch condition using TEV protease. Axin74–220 was then applied to a Superdex 75 size exclusion chromatography column (Amersham Pharmacia Biotech) for further purification and exchange of the buffer to the final NMR spectroscopy solution.

Backbone assignment and NMR spectroscopy titration. For NMR spectroscopy experiments, isotope-labeled axin74–220 was prepared in a mixture of 90% H_2O and 10% $2H_2O$ NMR spectroscopy buffer containing 25 mM sodium phosphate (pH 6.8), 300 mM sodium chloride, and 20 mM β-mercaptoethanol. All NMR spectroscopy experiments were performed at 298K on a Bruker DRX 600 MHz instrument equipped with a CryoProbe. Data were processed and analyzed using XWINNMR (Bruker Instruments), NMRPipe/NMRDraw (Biosym/Molecular Simulation Inc.), and Sparky software. Sequential resonance assignment was executed via ^{1}H-^{15}N heteronuclear single quantum coherence, three-dimensional (3D) HNCACB, and CBCACONH experiments. NMR titration experiments were performed with ^{15}N-labeled axin74–220 and KYA1797K using different molar ratios. The concentration of ^{15}N-labeled axin74–220 was 0.5 mM, and the molar ratios of ^{15}N-labeled axin74–220 to KYA1797K were 1:0, 1:1, 1:2, 1:3 and 1:4. The axin structure with PDB code 1DK8 was used to determine binding mode of axin74–220 and KYA1797K.

Fluorescence spectroscopy. Constants for binding between axin74–220 (WT or K147A) and the compounds (KYA1797K, IWR-1 or XAV939) were determined using a model RF-5301PC spectro-fluorephotometer (Shimadzu). All fluorescence spectroscopy experiments were performed in 25 mM sodium phosphate (pH 6.8), 300 mM sodium chloride and 20 mM β-mercaptoethanol; KYA1797K was titrated with axin74–220 protein up to ratios indicated in each figure legends in a thermostat cuvette. The dissociation constant (K_d) for KYA1797K with respect to axin74–220 binding was calculated using the following equation: $\log(F0 - F/F) = \log(1/K_d) + n \log[\text{ligand}]$, where F0 and F represent the fluorescence intensity of the protein at 322 nm in the absence and presence of the compound.

Patients and specimens. After analyzing *APC* mutational status, we randomly selected two unrelated FAP patients harboring an *APC* mutation and used them in this study. The cases were identified in the Department of Pathology at Yonsei University Medical Center between 2003 and 2005 for molecular marker studies. The specimens were freshly stored and obtained from the Cancer Specimen Bank of the National Research Resource Bank Program of the Korea Science and Engineering Foundation of the Ministry of Science and Technology. The Institutional Review Board of Yonsei Medical Center authorized these samples for use for research purposes. All tissue donors agreed to provide samples for this study. The differentiation grade of tumors was evaluated according to the guidelines of the American Joint Commission on Cancer (http://www.cancerstaging.org/). Each colon sample obtained from an FAP patient had more than 800 polyps[40]. For protein extraction, fresh tumor tissues were obtained immediately after surgical excision for available cases, and were stored at −80 °C before use.

Mutational analysis of *APC*. For analysis of germline mutations in the *APC* gene in FAP patients, peripheral blood lymphocytes were isolated from patient blood samples. Denaturing high-performance liquid chromatography (DHPLC) analysis was performed to determine the mutational status of all of the exons in the *APC* gene. All samples showing abnormal DHPLC patterns were analyzed by DNA sequencing.

Mutational analysis of *K-Ras*. For mutational analysis of *KRAS*, a QIAamp DNA Mini kit (Qiagen) was used to extract total genomic DNA from H&E-stained paraffin sections of 10-μm thickness containing a representative portion of each colorectal tumor block. A total of 50 ng of DNA was amplified in a 20-μl reaction solution containing 2 μl of 10× buffer (Roche), 1.7–2.5 mM $MgCl_2$, 0.3 μM primer pair (codon 12, 13, forward: 5′-TTATGTGTGACATGTTCTAAT-3′ and reverse: 5′-AGAATGGTCCTGCACCAGTAA-3′; codon 61, forward: 5′-TCA AGTCCTTTGCCCATTTT-3′ and reverse: 5′-TGCATGGCATTAGCAAAG AC-3′), 250 μM deoxynucleotide triphosphates and 2.5 units of DNA polymerase (Roche). Amplification was performed using a 5 min initial denaturation at 94 °C, followed by 30 cycles of 1 min at 94 °C, 1 min at 55 °C, and 1 min at 72 °C, and a 10 min final extension at 72 °C. PCR products were separated on a 2% agarose gel and purified using a QIAgen gel extraction kit (Qiagen) before being subjected to DNA sequencing analysis.

Denaturing high-performance liquid chromatography analysis. DHPLC was performed on a WAVE MD DNA fragment analysis system using a DNASep column (Transgenomic Inc.). DNA fragments bound to the DNASep column were eluted by altering the ratio of TEAA to acetonitrile. The eluted DNA molecules were detected by scanning with a UV-C detector. PCR products reannealed after denaturation were injected onto the column and eluted with a linear acetonitrile gradient at a flow rate of 0.9 ml/min, with a mobile phase consisting of a mixture of buffers A (0.1 M TEAA and 1 mM EDTA) and B (25% acetonitrile in 0.1 M TEAA).

Reporter assay for TOPflash or FOPflash. HEK293 cells were seeded at a density of 3×10^5 cells in a six-well plate. After 24 h, pTOPFLASH or pFOPFLASH[18] was transfected with a pCMV–β-galactosidase reporter. Twenty-four hours after the transfection, cells were treated with various concentrations of KY1220 with Wnt3a-CM or L-CM for 18 h, and were analyzed by luciferase assay. The cells were then harvested and lysed in 100 μl of Reporter Lysis Buffer according to the manufacturer's instructions. After centrifugation, 50 μl of the supernatant was used to measure luciferase activity and 20 μl of the supernatant was subjected to a β-galactosidase assay. Luciferase activity was normalized to the β-galactosidase activity.

Reverse transcription and quantitative real-time PCR. HEK293 cells were seeded at a density of 2×10^5 cells/well in 6-well plates and then treated with KY1220 dissolved in Wnt3a-CM. After 24 h of incubation, the cells were harvested, and total RNA was isolated using Trizol reagent (Invitrogen) according to the manufacturer's instructions. Total RNA (2 μg) was reverse-transcribed using 200 units of reverse transcriptase (Invitrogen) in a 20-μl reaction carried out at 42 °C for 1 h. The resulting cDNA (2 μl) was amplified in a 20 μl reaction mixture containing 10 mM dNTP (Takara), 10 pmol of the primer set (Bioneer), and 1 unit of Taq DNA polymerase (Invitrogen). The following primer sets were used: *CCND1*, forward 5′-GACCATCCCCCTGACGGCCGAG-3′ and reverse 5′-CGCACGTCGGTGGGTGTGC-3′; *MYC*, forward 5′-CATCATCATC CAGGACTG-3′ and reverse 5′-TGTTGCTGATCTGCTTCAGG-3′; *GAPDH*, forward 5′-ATTGTCAGCAATGCATCCTG-3′ and reverse 5′-GTAGGCCA TGAGGTCCACCA-3′. For quantitative real-time PCR analyses, the resulting cDNA (1 μl) was amplified in 10 μl of iQ SYBR Green Supermix (Bio-Rad). The comparative cycle-threshold (C_T) method was used, and *GAPDH* served as an endogenous control. The following primer sets were used: *CTNNB1* (which encodes β-catenin), forward 5′-ACAAGCCACAAGATTACAAGAA-3′ and reverse 5′-GCACCAATATCAAGTCCAAGA-3′; *HRAS*, forward 5′-GGAAG CAGGTGGTCATTG-3′ and reverse 5′-AGACTTGGTGTTGTTGATGG-3′; *NRAS*, forward 5′-AAGAGTTACGGGATTCCATTC-3′ and reverse 5′-CCA TCATCACTGCTGTTGA-3′; *KRAS*, forward 5′-AAACAGGCTCAGGACTT AG-3′ and reverse 5′-GTATAGAAGGCATCATCAAC-3′; *GAPDH*, forward 5′-CTGGTAAAGTGGATATTGTTG-3′ and reverse 5′-TGGAAGATGTGA TGGGATTT-3′.

Testing of KYA1797K specificity. A Cignal Finder Multi-Pathway Reporter Arrays kit (Qiagen) was used to test the specificity of KYA1797K with respect to regulation of the Wnt/β-catenin and Ras/ERK signaling pathways. Cancer-related pathways were monitored, including Wnt/β-catenin, MAPK/ERK, Notch, p53/DNA damage, TGFβ, cell cycle/pRb-E2F, NF-κB, Myc/Max, hypoxia and MAPK/JNK. HEK293 cells (5×10^4 cells/well) were transfected with 2 μg of plasmid/well in a 96-well plate using SureFECT reagent (Qiagen). After transfection and seeding, KYA1797K (5 μM) was added, and the cells were incubated for 12 h, after which the plates were analyzed for firefly luciferase activity. The luciferase signals were normalized to *Renilla* luciferase activity as an internal control. All of the materials and methods followed the protocol described by the manufacturer.

Generation of axin mutants. The residues leucine 92, aspartate 94, isoleucine 99, leucine 115, phenylalanine 119, glycine 123, lysine 126 and lysine 147 of axin-WT-V5 (encoded within pDEST40-Axin1) were changed to alanine by mutagenesis following the Quikchange site-directed mutagenesis protocol (Stratagene) using primers (**Supplementary Table 2**). All the primers were obtained from Bioneer and the mutations were confirmed by DNA sequencing analysis (Cosmo Genetech).

Biochemical assays for tankyrase 1 and 2. Tankyrase auto-PARsylation biochemical assays were conducted to measure the effects of KYA1797K or XAV939 on tankyrase 1 and 2 activity. Increasing concentrations of the compounds (0.0016 μM, 0.008 μM, 0.04 μM, 0.2 μM, 1 μM, 5 μM and 25 μM) were incubated with tankyrase 1 (2 μg) or tankyrase 2 (1 μg) for 1 h and chemiluminescence was evaluated. The chemiluminescence values were normalized to DMSO-treated positive control. All the materials and methods for measurement of tankyrase activity were performed according to the manufacturer's protocol (BPS bioscience).

General methods for chemistry. Full experimental details and characterization data for all new compounds are included in the **Supplementary Note**. Information about KYA1797K is summarized in **Supplementary Table 3**.

Pharmacophore generation. Six active compounds (KY1220, KYA2370, KYA1797, KYA1797K, KYA1690 and KYA1690K (**8**)) were used to generate pharmacophores as a type of ligand-based drug design. HipHop5 approach in Discovery Studio 3.1 (Accelrys, Inc.) was used to produce common feature pharmacophores required for binding. Ten hypotheses were generated by HipHop, and the best HipHop pharmacophore hypothesis involved a phamacophore containing four common features: one hydrophobic group on either the pyrrole or furan ring, and three hydrogen bond acceptors (the oxygen of the 4-nitrophenyl group, the oxygen of the rhodanine or thiohydantoin group, and the oxygen of the carboxylic acid). The highly ranked hypothesis, the molecule of which best mapped onto the proposed pharmacophores, was selected for further validation. The fit values of the generated pharmacophores and TOPflash inhibitory activity showed good correlation with KYA1690, KYA2370 and KYA1797, which displayed the best *in vitro* assay results. However, the lead compound KY1220 did not fit well on the pharmacophores despite its good inhibitory activity. This result can be explained by the distance between each of the pharmacophores. The thiohydantoin sulfur fits in the hydrogen bond acceptor pharmacophore instead of the oxygen of the carboxylic acid when a compound, such as the lead compound, lacks a carboxylic acid moiety. However, the distance between the thiohydantoin sulfur and the hydrophobic group was 7.64 Å, which was a much shorter distance than that between the oxygen of the carboxylic acid and the hydrophobic group, which was 9.79 Å. They shared the same hydrogen bond acceptor pharmacophore but the difference in distance led to a variation in fit value on the pharmacophores. The distance between each pharmacophore also affected the carbon chain length of the carboxylic acid, which was substituted to increase solubility. The comparatively short acetic acid and long hexanoic acid substituted compounds displayed low fit values on the pharmacophores.

Solubility testing. High-performance liquid chromatography (HPLC) was performed to assess the solubility of our compounds. Samples of the analogs equivalent to 1.5 mg of KY1220 were added to approximately 1.5 ml of distilled water (DW) or PBS, sonicated for 15 min, and shaken horizontally. The samples were then filtered through a hydrophilic GHP membrane filter with 0.2-μm pore size, stored frozen for 2–3 d, and then freeze-dried. Each sample was then dissolved completely in methanol or DMSO at a concentration of 500 μg/ml. We used caffeine as an internal standard at a concentration of 50 p.p.b. An aliquot of the serially diluted suspension was collected and used for the HPLC assay after filtration again through a GHP membrane. The assay was performed on a Shimadzu LC-20A HPLC system using an Agilent XDB-C18 column (250 mm × 4.6 mm inner diameter; particle size 5 μm; Agilent Technologies). The detection wavelength was 254 nm. The mobile phase was 20%/0.05% formic acid in H_2O/0.05% formic acid in acetonitrile at a flow rate of 1 ml/min. The injection volume was 3 μl. KYA1690 and KYA2370 in DW were not detected using HPLC, indicating that the compounds were completely insoluble. KYA1797 was detected at a concentration over 500 μg/ml using HPLC, but undissolved particles were still visible. Therefore, in order to increase the solubility of the compounds without affecting their structures, the compounds were formulated as potassium salts. The salt form of the compounds dissolved well in DW; however, there was no improvement in solubility in PBS, which is a more relevant solvent for use in *in vivo* models (**Supplementary Table 4**). Tween 80 was therefore added to the PBS at a concentration of 10% to increase the solubility of the compounds.

Chemical probes. To identify targets for KYA1797K, KYA2406 (**10**) and LJE-H-226 (**11**), two analogs of KYA1797 were synthesized in biotin-conjugated form. Initially, KYA1797 was biotinylated at the carboxylic acid group. However, the biotinylated compounds inhibited TOPflash reporter activity only very weakly. Because the biotin was introduced on a carboxylic acid moiety, a crucial part of the molecule with respect to solubility, biotinylated KYA1797 exhibited solubility problems and subsequent low inhibition of TOPflash reporter activity. Therefore, to improve the solubility and efficacy of the biotinylated compounds, KYA1690 was used in place of KYA1797 and the rhodamine moiety of KYA1690 was substituted with a 2,4-thiazolidinedione moiety, producing a 2,4-thiazolidinedione compound. Based on the 2,4-thiazolidinedione compound, we synthesized a biotinylated active compound (LJE-H-225).

Statistical analysis. All data are expressed as the mean ± s.d., and the number of samples is indicated in each figure legend. The statistical significance of differences was assessed using the Student's *t*-test or ANOVA. Results shown are representative of at least three independent experiments. Significance was accepted at $P < 0.05$.

33. Yun, M.S., Kim, S.E., Jeon, S.H., Lee, J.S. & Choi, K.Y. Both ERK and Wnt/beta-catenin pathways are involved in Wnt3a-induced proliferation. *J. Cell Sci.* **118**, 313–322 (2005).
34. Hoeflich, K.P. *et al.* Requirement for glycogen synthase kinase-3beta in cell survival and NF-kappaB activation. *Nature* **406**, 86–90 (2000).
35. Mo, H. & Elson, C.E. Apoptosis and cell-cycle arrest in human and murine tumor cells are initiated by isoprenoids. *J. Nutr.* **129**, 804–813 (1999).
36. Kim, M.Y., Kaduwal, S., Yang, D.H. & Choi, K.Y. Bone morphogenetic protein 4 stimulates attachment of neurospheres and astrogenesis of neural stem cells in neurospheres via phosphatidylinositol 3 kinase-mediated upregulation of N-cadherin. *Neuroscience* **170**, 8–15 (2010).
37. Ha, N.C., Tonozuka, T., Stamos, J.L., Choi, H.J. & Weis, W.I. Mechanism of phosphorylation-dependent binding of APC to beta-catenin and its role in beta-catenin degradation. *Mol. Cell* **15**, 511–521 (2004).
38. Kim, S. & Jho, E.H. The protein stability of Axin, a negative regulator of Wnt signaling, is regulated by Smad ubiquitination regulatory factor 2 (Smurf2). *J. Biol. Chem.* **285**, 36420–36426 (2010).
39. Kolligs, F.T., Hu, G., Dang, C.V. & Fearon, E.R. Neoplastic transformation of RK3E by mutant beta-catenin requires deregulation of Tcf/Lef transcription but not activation of c-myc expression. *Mol. Cell. Biol.* **19**, 5696–5706 (1999).
40. Winawer, S. *et al.* Colorectal cancer screening and surveillance: clinical guidelines and rationale-Update based on new evidence. *Gastroenterology* **124**, 544–560 (2003).

doi:10.1038/nchembio.2103